Int. J. Electrochem. Sci., 14 **(2019)** 8557 – 8568, doi: 10.20964/2019.09.05

International Journal of
ELECTROCHEMICAL
SCIENCE
www.electrochemsci.org

Electrolytic Refining of High Carbon Ferrochromium to Produce Pure Ferrochromium in NaCl-KCl Melt

Qian Kou[1,2], Weiliang Jin[1,2], Guolong Liu[1,2], Meichen Wang[1], Saijun Xiao[1,2,]*

[1] School of Metallurgy Engineering, Anhui University of Technology, Maanshan, Anhui, China, 243002;
[2] Key Laboratory of Metallurgical Emission Reduction & Resources Recycling, Anhui University of Technology, Maanshan, Anhui, China, 243002.
[*]E-mail: jxddroc@126.com

Received: 13 April 2019 / *Accepted:* 20 June 2019 / *Published:* 31 July 2019

In this paper the electrolytic refining of remelted high carbon ferrochromium (HCCrFe) to produce pure ferrochromium in molten salts was investigated. The remelted HCCrFe was employed as the working electrode, tungsten as the counter electrode, and Ag/AgCl as the reference electrode, to establish a three-electrode cell. Potentiostatic electrolysis (anode potential, 0.3 V vs Ag/AgCl) was conducted in NaCl-KCl melt at a temperature of 710℃. The cathode product was examined by x-ray diffraction (XRD), elemental analysis and x-ray photoemission spectroscopy (XPS). The results indicate that pure ferrochromium with low contents of C, S, and P has been successfully prepared by this method. In addition, the left anode residue was also characterized by scanning electron microscopy (SEM) and energy disperse spectrum (EDS), exhibiting porous appearance with a large amount of carbon contained. Subsequently, galvanostatic electrolysis was performed with different current densities (0.33 A·cm^{-2}, 0.50 A·cm^{-2}, 0.58 A·cm^{-2} and 0.66 A·cm^{-2}). The composition and microstructure of the deposited ferrochromium under these different conditions were analyzed by XRD and SEM. It is found that with the increase of current densities, the particle size of cathode product becomes coarser and tends not to be oxidized.

Keywords: high carbon ferrochromium, pure ferrochromium, electrolytic refining, molten salts

1. INTRODUCTION

With the increasing requirements for the purity of steel, the development of new process for refining of ferroalloy has been explored, to reduce the effect of undesired elements contained in the ferroalloy, which is added as an alloying agent during the end of steel making [1-3]. To meet the requirements for the impurities content in the special steels, such as high Cr stainless steel, acid-resistant

steel and heat-resistant steel, and to substitute the employment of expensive metal Cr as the alloying agent in steel plants, it is of significant importance to develop a new type of pure ferrochromium product with low cost [4-8].

Currently, traditional processes to prepare low carbon ferrochromium mainly include electrothermal silicon reduction, off-furnace blending, and solid decarbonization under vacuum. However, the product from these processes, with unstable quality, can not meet the requirements for production of special steels [9]. Recently, a process consisting of three steps including ball milling and pelletizing of mixture of high carbon ferrochromium (HCCrFe) and pure Cr_2O_3, decarbonization under vacuum in electric furnace and refining by induction furnace remelting, has been reported [5,6]. Nevertheless, due to its complex process and inefficient removal of inclusions, the replacement of using metal Cr by the produced ferrochromium from this process could not be achieved.

Molten salt electrorefining is a potentially promising method to refine HCCrFe to produce pure ferrochromium due to its good characteristics. Actually, in 1969 Cattoir and Sullivan [10] reported the feasibility of preparation of high-purity chromium by electrorefining of HCCrFe in molten salts, but the separation of Cr and Fe was not easily realized. In 1977 Suri and Gupta [11] investigated molten salt electrolysis for the production of pure chromium metal from its carbide and aluminothermically reduced form. The electroplating of Cr from fused fluoride and chloride electrolytes by direct and periodically reverse plating has also been studied [12-15]. Chen and Gordo [16,17] also extracted chromium powder of high purity from Cr_2O_3 by an electrolytic process in molten salts. Ge and his coworkers [18] applied this Fray-Farthing-Chen Cambridge process on the production of ferrochromium from chromium and iron oxide and chromite ore, respectively, in molten $CaCl_2$. The authors have investigated the feasibility of electrorefining of high carbon ferromanganese (HCMnFe) to produce pure ferromanganese and hierarchical porous carbon in molten salts [19]. Recently, the electrochemical behavior of Cr^{2+} in molten NaCl-KCl on different working electrodes has also been studied by the authors [8,20]. In this work, HCCrFe is employed as the anode to produce pure ferrochromium on the cathode under electrolysis in NaCl-KCl molten salts. It is expected that the produced ferrochromium could replace the current alloying agent Cr in steel plants. The availability of this process is investigated and the effect of current densities on the composition and morphology of cathode product is discussed.

2. EXPERIMENTAL

Reagents of the experiments are NaCl and KCl, which are analytic reagent. The mixture of NaCl-KCl molten salts (mole ratio, 50.6:49.4) was dried under blast oven for more than 48h at 200℃ to remove excess water. Raw HCCrFe was remelted at 1580℃ for 4h under argon atmosphere to make its composition more uniform. Excess carbon powder was added in this procedure to prevent oxidation of HCCrFe. The sample was removed after the furnace temperature cooled down to room temperature.

All the electrochemical experiments were performed in an alumina crucible located in an electric furnace under pure argon atmosphere (99.99%), with the experimental setup shown in Fig. 1. During potentiostatic electrolysis, a three-electrode cell was applied. The working electrode was a HCCrFe plate

(3×5×50mm; 7.54 mass% C contained), and tungsten wire with a diameter of 1mm was selected as the counter electrode. The Ag/AgCl electrode was used as the reference electrode, which consists of a mullite tube containing a silver wire, immersed in NaCl-KCl melt containing 2.0 mass% AgCl inside the mullite tube. During galvanostatic electrolysis, a two-electrode cell was employed with different applied currents. The HCCrFe plate and tungsten wire were used as the anode and cathode, respectively. After electrolysis, all electrodes were raised above the electrolyte level. After the furnace temperature cooled down to room temperature, the collected cathode product were washed in deionized water to remove salts, followed in the acetone to remove the additional water and dried in a vacuum oven.

Both of the electrochemical measurement (cyclic voltammetry) and electrolysis with a three-electrode cell were performed by PARSTAT 2273 potentiostat with Powersuite software (Princeton Applied Research, AMETEK). Cyclic voltammetry was applied to study the reduction process of Cr^{2+} at a scan rate of 100 $mV \cdot s^{-1}$. Electrolysis with a two-electrode cell was carried out with a DLCC5000L (IUX. Power) DC regulated power source. The composition and microstructure of deposits on the cathode were characterized by x-ray diffraction and scanning electron microscopy, respectively. The carbon and sulphur analyzer and plasma emission spectrometer were used to measure the contents of C, S and P in the product. X-ray photoemission spectroscopy (XPS) was used to determine the main existing forms of carbon in the product.

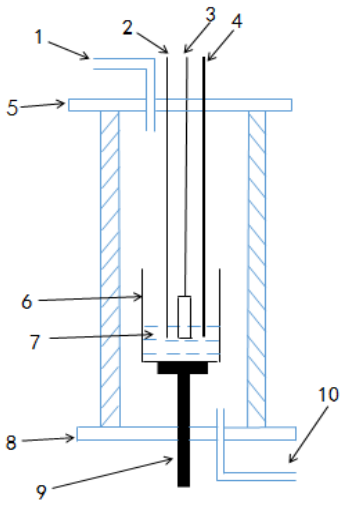

1. argon gas inlet;
2. counter electrode;
3. working electrode;
4. reference electrode;
5. cover flange;
6. alumina crucible;
7. NaCl-KCl melt;
8. bottom flange;
9. stainless steel supporting rod;
10. argon gas outlet.

Figure 1. Experimental schematic for electrochemical tests.

3. RESULTS AND DISCUSSION

3.1 Electrochemical tests

The electrochemical tests were carried out to investigate the dissolution of HCCrFe. The electrochemical window of the selected electrolyte was demonstrated in Fig. 2. Tungsten was used as the working electrode, carbon as the counter electrode, and Ag/AgCl as the reference electrode, for cyclic voltammetry tests in NaCl-KCl molten salts at a temperature of 710℃. In Fig. 2(a), positive to the deposition potential (around -2.0 V vs Ag/AgCl) of alkali metals, there is no faradic reaction. Then HCCrFe and glassy carbon were employed as the working electrodes, for the tests of anodic polarization. The polarization curves of HCCrFe (solid line) and glassy carbon (dotted line) are illustrated in Fig. 2(b), with a scan range from open circuit potential to 1.2 V vs Ag/AgCl. It is seen that no current is recorded before the evolution of chlorine (1.1 V vs Ag/AgCl) using glassy carbon, while obvious current is recorded using HCCrFe. The current density rises when the scanning potential shifts positively, which indicates the occurrence of anode dissolution of HCCrFe in NaCl-KCl melt. Anode potential of 0.3 V vs Ag/AgCl was selected as the value for potentiostatic electrolysis of HCCrFe.

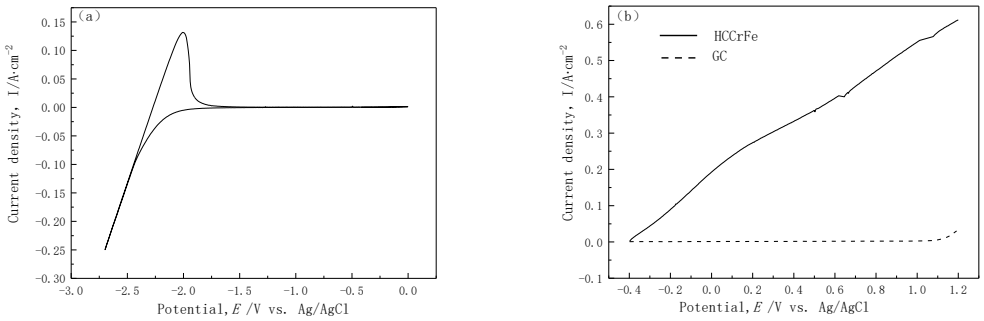

Figure 2. (a): Cyclic voltammogram on tungsten in NaCl-KCl molten salts at 710℃; (b): Anode polarization curves of high carbon ferrochromium and glassy carbon in NaCl-KCl molten salts at 710℃.

3.2 Potentiostatic electrolysis

Based on the electrochemical tests, potentiostatic electrolysis with an applied anode potential of 0.3 V was carried out. The dependence of current on anode potential is shown in Fig. 3. The electrolysis lasted for around 20h. During the electrolysis, the value of the current is relatively stable in the range of 70-90 mA.

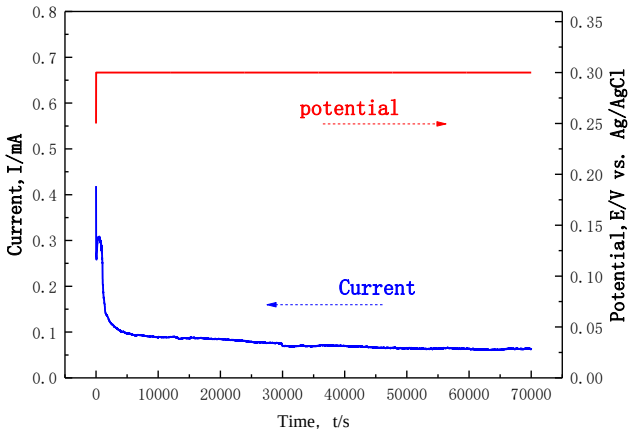

Figure 3. Current–time plot recorded during the potentiostatic electrolysis of high carbon ferrochromium under 0.3 V vs Ag/AgCl for 20h in NaCl–KCl melt at 710℃.

3.2.1 Cathode product

The appearance of the cathode product after rinsing and drying is shown in Fig. 4(a). The product mainly consists of powder, exhibiting black appearance. Fig. 4(b) presents the SEM image of the product, which mainly consists of small particles, with the size less than 2 um.

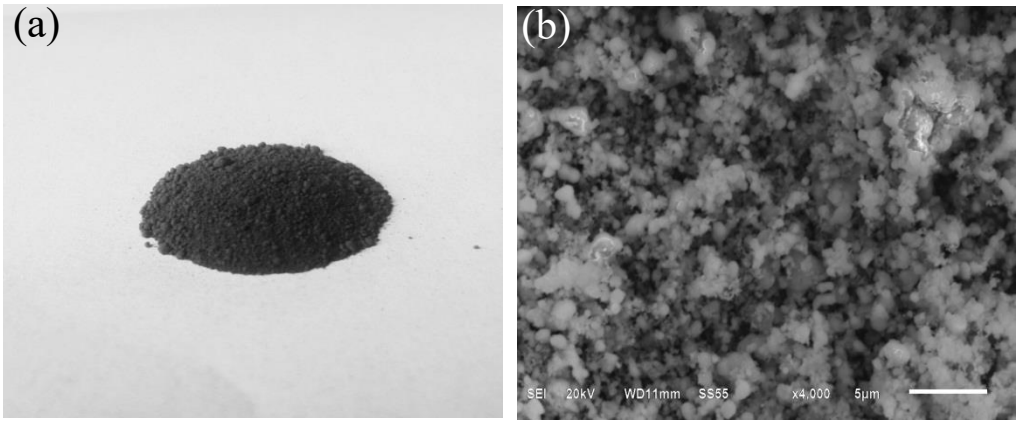

Figure 4. Photo (a) and SEM image (b) of cathode deposit under 0.3 V vs Ag/AgCl for 20h in NaCl–KCl melt at 710℃.

The XRD patterns of the HCCrFe before electrolysis and cathode product are demonstrated in Fig. 5. Fig. 5 (a) shows that the feeding material is composed of Cr_3C_7, Fe_3C and C. Lesko [21] presented the existence of Cr_7C_3 in slowly cooled HCCrFe. Fig. 5 (b) shows that the cathode product is ferrochromium. Therefore, during the electrolysis, it is considered that Cr and Fe in the anode dissolved into the melt to form Cr and Fe ions, which migrated to the cathode to be reduced as ferrochromium. Meanwhile, the carbon was left in the anode.

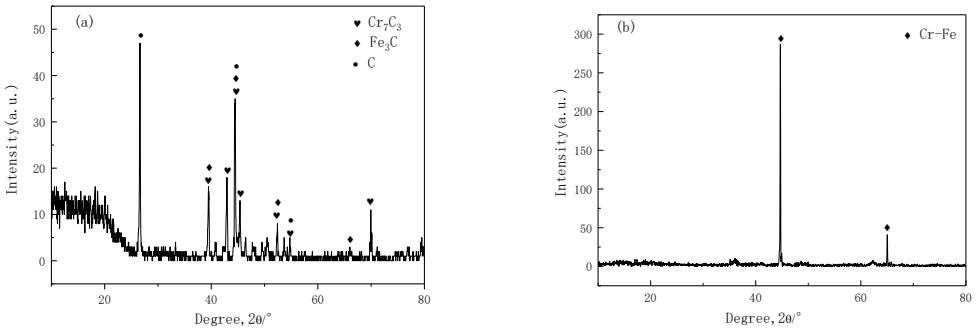

Figure 5. (a): The XRD patterns of the HCCrFe before electrolysis; (b): XRD result of the cathode product under 0.3 V vs Ag/AgCl for 20h in NaCl–KCl melt at 710℃.

The deposit with a weight of 1.8g, was analyzed to determine the contents of C, S and P, illustrated in Table 1. It is found that the contents of C, S and P are 0.453 mass %, 0.0089 mass% and less than 0.008 mass%, respectively. The carbon content is greatly reduced compared with that in the HCCrFe (7.54 mass%) before electrolysis and the contents of S and P are low enough, which meet the requirements for low carbon ferrochromium.

During several repeated experiments, a small amount of carbon was always detected in the cathode product. X-ray photoemission spectroscopy (XPS) was used to study the main existing forms of carbon in the product. The result of high-resolution XPS spectra of C1s excitation was as shown in Fig. 6. The spectra were deconvoluted into four components adopted in the analysis of carbon materials [22-25]. Four peaks at the binding energy of 284.7eV, 285.9eV, 286.8eV and 288.3eV can be assigned to C-C (carbon atoms of aromatic network in graphite), C-O, C=O and -O-C=O groups. Therefore, it is concluded that the carbon in the cathode product mainly exists in an elemental state. The minor existence of functional groups containing C and O could be due to the contact with some organics. In addition, the binding energy of C-Cr was reported to be 282.8 eV, about 2 eV lower than C-C bond [26]. The binding energy of C-Fe was reported to be 283.3 eV, about 0.8 eV lower than C-C bonds [27]. These reported results further confirms the absence of carbides with Cr or Fe. The presence of carbon is probably due to the falling of a small amount of loose anode residue into the melt after electrolysis, which contained a large amount of carbon after dissolution of Cr and Fe. The collected product could be contaminated by the fallen anode residue.

Table 1. The contents of trace elements (C, S, P) in the cathode product obtained by potentiostatic electrolysis at 0.3V (vs Ag/AgCl) for 20h in NaCl–KCl melt at 710℃.

Elements	Results(mass %)	Test methods
C	0.453	GB/T 20123-2006
S	0.0089	GB/T 20123-2006
P	<0.008	GB/T 4699.3-2007*

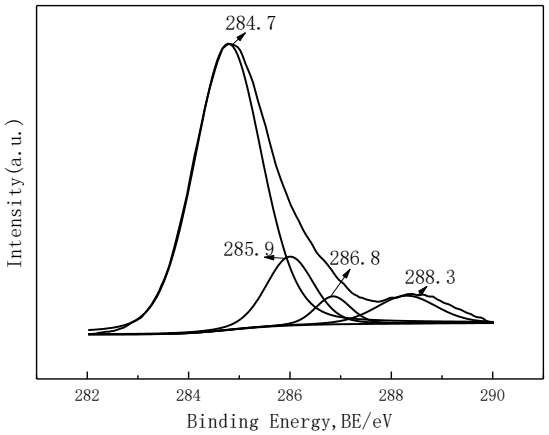

Figure 6. C1s XPS spectra of deposits obtained by potentiostatic electrolysis at 0.3V (vs Ag/AgCl) for 20h in NaCl–KCl melt at 710℃.

Another experiment was carried out to confirm the above assumption. In this case, only the cathode product near the cathode was recovered and analyzed by carbon and sulphur analyzer, while the cathode product near the anode was abandoned. The results show that in this time the carbon and sulphur contents of are 0.26 mass% and 0.0017 mass%, respectively. The incomplete removal of carbon could be due to relatively small distance of anode and cathode in the electrolytic cell. A larger distance between anode and cathode can further reduce the impurity in the cathode product.

3.2.2 Anode residue

The composition of the anode residue (HCCrFe after electrolysis) is determined by XRD, as illustrated in Fig. 7. It is observed that compared with the raw material, the peak intensity of Cr_7C_3 and Fe_3C is greatly reduced, implying that most of the Cr and Fe are oxidized into the electrolyte. Fig. 8(a) and (b) show the microstructures of the anodes before and after electrolysis. From Fig. 8(a), three phases including dark grey, grey and light grey phases, were seen. Table 2 gives the corresponding elemental analysis by EDS in their different areas. It is found that the dark grey phase is mainly composed of around 14 mass% C, 62 mass % Cr and 24 mass % Fe, the light grey phase is mainly composed of around 6 mass% C, 13 mass % Si and 6 mass % Cr and 75 mass % Fe, and the composition of the grey phase is between that of the two phases. In Fig. 8(b), the anode after electrolysis is loose and porous. Table 3 presents the corresponding composition by EDS. The content of carbon increased greatly and the content of Cr and Fe reduced significantly. These results are in agreement with the XRD results.

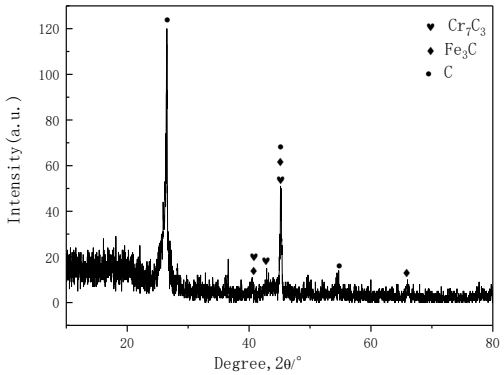

Figure 7. The XRD patterns of the anode after potentiostatic electrolysis at 0.3V (vs Ag/AgCl) for 20h in NaCl–KCl melt at 710℃.

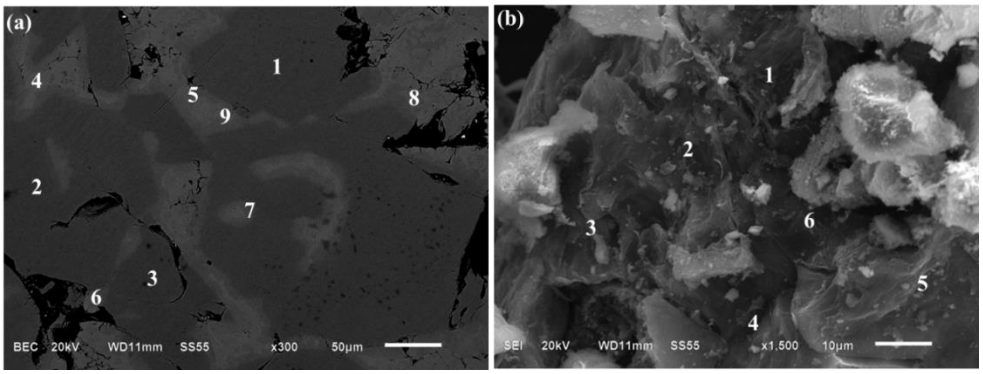

Figure 8. The SEM images of HCCrFe before (a) and after (b) electrolysis.

Table 2. The main elements contents of HCCrFe before electrolysis.

Area	1	2	3	4	5	6	7	8	9
C(mass%)	14.05	14.94	14.75	6.79	6.04	7.99	10.50	10.68	10.84
Si(mass%)	0	0	0	12.89	13.32	12.35	9.41	9.71	9.46
Cr(mass%)	60.98	62.79	61.01	5.59	5.54	6.63	34.47	31.94	28.69
Fe(mass%)	24.97	22.27	24.24	74.18	75.10	73.04	45.62	47.67	51.00

Table 3. The main elements contents of HCCrFe after electrolysis.

Area	1	2	3	4	5	6
C (mass%)	86.74	84.07	81.36	73.49	71.62	81.68
Si (mass%)	0.45	0.77	0.89	3.56	2.13	1.94
Cr (mass%)	9.13	10.32	11.25	15.04	15.78	12.33
Fe (mass%)	3.68	4.48	6.5	7.91	10.47	4.05

Some interesting morphologies were also found in the left anode residue. Fig. 9 demonstrates two of the typical microstructures. By EDS analysis, shown in Table 4, the main composition is carbon, with minor Fe and Cr. Thus in these areas there are carbon sheets left. The formed pores consists of voids between carbon sheets, with a relatively uniform pore size. According the authors' previous work [19] on electrorefining of HCMnFe, the left anode was composed of hierarchical porous carbon, which could be potentially applied in the field of supercapacitors. Therefore, in this work, the existence of this type of carbon sheets could also provide an alternation for preparation of porous carbon for application of supercapacitors.

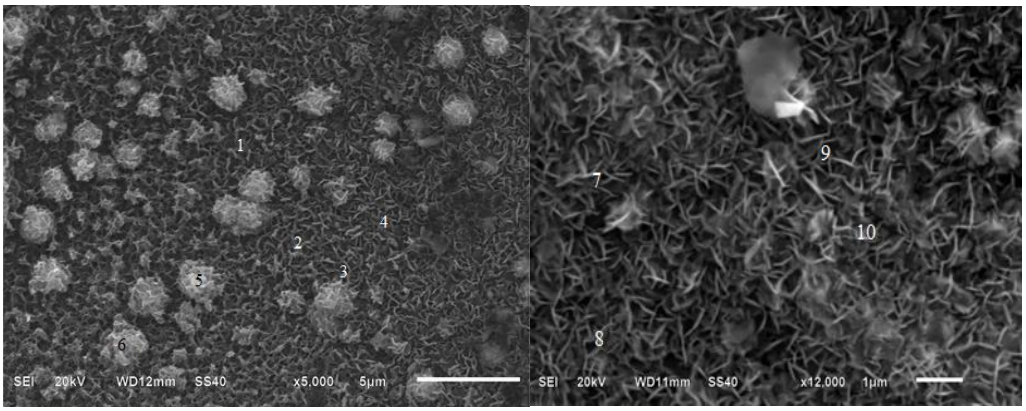

Figure 9. The SEM images of microstructures of the anode after electrolysis.

Table 4. The main elements contents of the anode after electrolysis in Figure 9.

Area	1	2	3	4	5	6	7	8	9	10
C(mass%/mol%)	100	100	94.81 98.84	94.14 98.68	71.32 91.73	66.90 89.98	93.49 98.53	92.36 98.25	95.12 98.91	93.719 8.58
Cr(mass%/mol%)	0	0	0	0	15.85 4.71	21.096 .55	0	0	0	0
Fe(mass%/mol%)	0	0	5.19 1.16	5.86 1.32	12.83 3.56	12.013 .47	6.51 1.47	7.64 1.75	4.88 1.09	6.29 1.42

3.3 Galvanostatic electrolysis

The effect of electrolysis current on cathode product composition and morphology was investigated. Different currents (100mA, 200mA, 300mA and 400mA) were applied on the cell under galvanostatic mode, with the electrolysis time lasting for 10h, respectively. The cathode product is examined by XRD, with the patterns shown in Fig. 10. The XRD results demonstrates that the deposited ferrochromium contains a small amount of Cr_2O_3. With the increase of the current density, the diffraction peak intensity of Cr_2O_3 is gradually reduced. At a current density of 0.66 $A \cdot cm^{-2}$, pure ferrochromium was obtained without containing Cr_2O_3. In addition, the cathode products obtained under different currents were examined by SEM, with the microstructure presented in Fig. 11. It is seen that the products

under various conditions are particles. The morphology are not greatly affected by the different applied currents. With the rise of the current density, the particle size increases.

According to the formula (1) [28], it can be seen that the increase of the concentration of metal ions in the electrolyte causes less presence of nuclei (Nn), thus benefiting the growth of nuclei and formation of coarse particles. Low concentration could result in serious concentration polarization and high overpotential. So the nucleating current density is larger than the crystal–growing current density, and the growth of the crystal is restricted, resulting in existence of more nuclei without growing up. In addition, serious polarization lead to thick diffusion layer, and the crystals grow nonuniformly and loosely. High concentration lowers concentration polarization and overpotential, and the growth of the crystal is favored, resulting in bigger size of particles [29]. Liu [30] and Weng [31] reported the similar results in their investigation of deposition of titanium in molten NaCl-KCl-TiClx.

$$N_n = a + b \times \lg[D_k/C_{me}] \quad (1)$$

Where N_n is number of crystal nucleation, a, b are constants dependent on the properties of the metal, D_k is cathode current density and C_{me} is the concentration of metal ions in the electrolyte.

In this experiment, the feeding Cr ions are not introduced from addition of soluble raw materials into the melt, but from the dissolution of HCCrFe anode. Therefore, it is assumed that increasing the current density could result in acceleration of anode dissolution of HCCrFe, thus increasing the concentration of metal ions in the molten salts. It might be that the effect of concentration of metal ions is dominant, leading to the increase of the particle size of the cathode products with the increasing current density.

Combining the results of XRD and SEM, it is found that the larger particle size of the product corresponds to less oxidation. At lower current density, the sample exhibits finer size and more serious oxidation. It is probably due to that the finer powder tends to be oxidized more easily when contacting with water during the collection procedure.

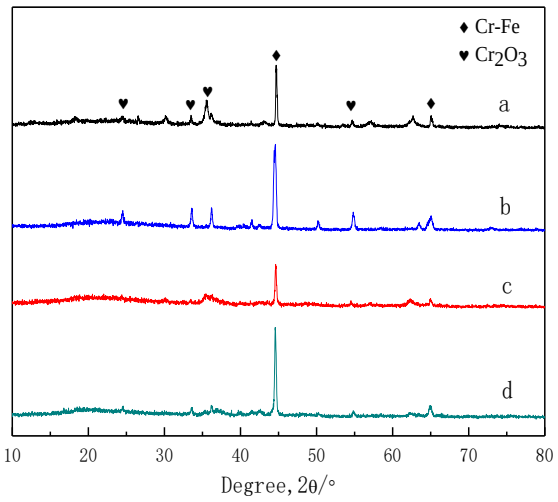

Figure 10. XRD patterns of the cathode products at different cathode current densities for 10h in NaCl–KCl melt at 710℃. (a): 0.33 A·cm^{-2}; (b): 0.5 A·cm^{-2}; (c): 0.58 A·cm^{-2}and (d): 0.66 A·cm^{-2}.

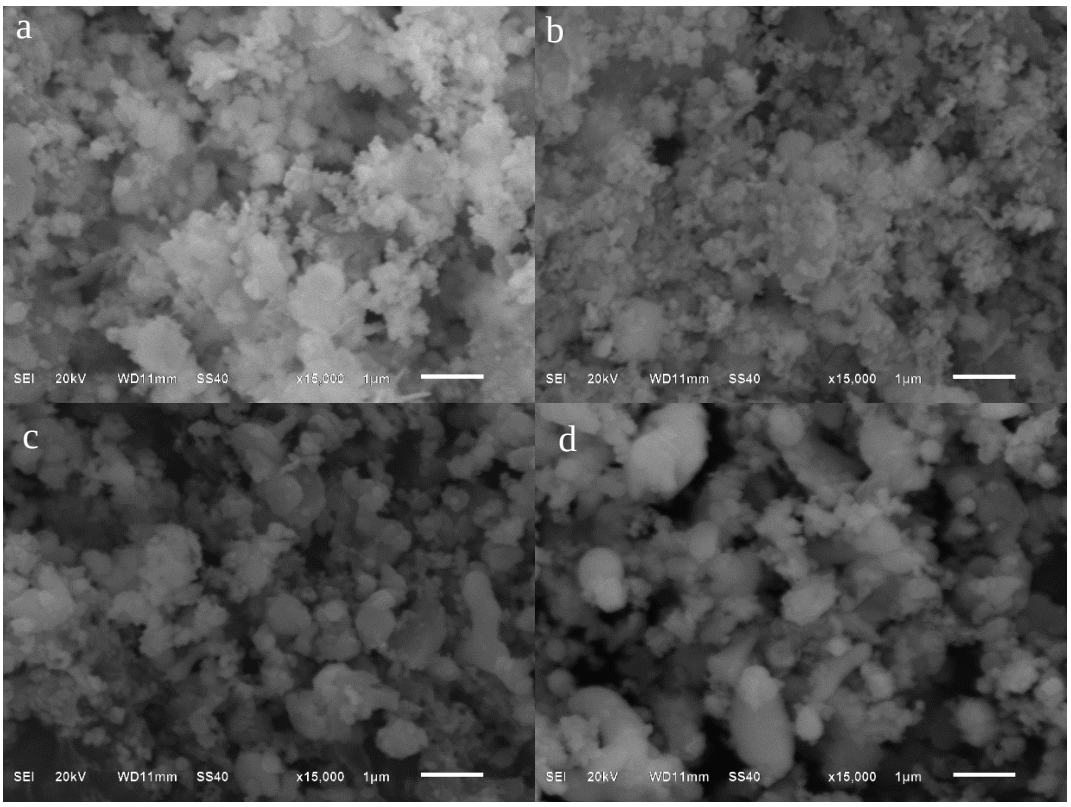

Figure 11. SEM images of the cathode deposits at different cathode current densities for 10h in the NaCl–KCl melt at 710℃. (a): 0.33 A·cm^{-2}; (b): 0.5 A·cm^{-2}; (c): 0.58 A·cm^{-2} and (d): 0.66 A·cm^{-2}.

4. CONCLUSIONS

High carbon ferrochromium was used as the anode to produce pure ferrochromium at the cathode by molten salt electrolysis. Both potentiostatic and galvanostatic electrolysis were carried out in molten NaCl-KCl system at a temperature of 710 ℃. The main conclusions are as follows:

(1) Pure ferrochromium was successfully produced with low contents of C, S, and P (0.26 mass%, 0.0017 mass% and less than 0.008 mass%). The existing state of C contained in the cathode deposit is mainly elemental form. The content of impurities is greatly affected by collection procedure of the cathode products. Meanwhile, the remained anode is porous, with a large amount of carbon, and also exhibits some interesting morphology of carbon sheets.

(2) In galvanostatic electrolysis with various current densities, it is found that with the rise of the current density, the particle size of the deposits become coarser and the product tends not to be oxidized.

ACKNOWLEDGEMENTS
This research was financially supported by National Natural Science Foundation of China (51404001), Anhui province overseas scholars innovation project funding program (2017) and Student research training funding program of Anhui province (201710360144).

References

1. J. Safarian and L. Kolbeinsen, Purity Requirements for Mn Alloys for Producing High Manganese TRIP and TWIP Steels, *Ukrainian Association of Ferroalloys*, Almaty, Kazakhstan (2013)175-182.
2. S. J. Chu and Q. Niu, *Ferro-alloys*, 2(2002) 41-46.
3. L. Wang, J. Chen, J. J. Hao, W. M. Lin, and Y. G. Deng. *Chin. J. Process. Eng.*, 13(2013) 415-423.
4. Y. I. Voronov, V. N. Karnoukhov and E.N. Akimov, *Russ. Metall*, 2011(2011) 1131-1133.
5. L. Hu, J. X. Chen and J. R. Peng, Chromium resource and advanced ferrochromium. Chemical Industry Press, Beijing, China, 2010.
6. W. S. Guo and W. X. He, 2010.04.28. CN 101698920.
7. K. L. Wu, L. Li, H. B. Zhu, J. H. Peng, L. B. Zhang and L. Q. Dai, *Powder Metall. Ind*., 25(2015) 22-25.
8. W. Liu, G. L. Liu, S. J. Xiao and J. Zhang, *Int. J. Electrochem. Sci*., 12(2017) 1589-1599.
9. H. Weitz and A. M. Garberscraig, *Process. Extr. Metall. Rev.*, 37(2016) 186-178.
10. K. P. V. Lei, F. R. Cattoir and T.A. Sullivan, *J. Electrochem. Soc.*, 120(1973) 211-215.
11. A. K. Suri and C. K. Gupta, *Surf. Technol.*, 5(1977) 271-276.
12. J. F. Smith, *Thin Soild Films.*, 95(1982) 151-160.
13. R. A. Bailey, *J. Appl. Electrochem*, 16(1986) 737-744.
14. T. Vargas and D. Inman, *J. Appl. Electrochem*, 17(1987)2 70-282.
15. A. Cotarta, J. Bouteillon, T. C. Poignet, F. Vasiliu and V. Cotarta, *J. Appl. Electrochem*, 31(2001) 987-995.
16. G. Z. Chen, E. Gordo and D. J. Fray, *Metall. Mater. Trans.*, B35(2004) 223-233.
17. E. Gordo, G. Z. Chen and D. J. Fray, *Electrochim. Acta*., 49(2004) 2195-2208.
18. X. Ge, S. Jin, M. Zhang, X. Wang and S. Seetharaman, *Metall. Sect. B-Metall*, 51(2015) 185-191.
19. W. Liu, G. L. Liu, Q. Kou and S. J. Xiao, *Rsc. Adv.*, 7(2017) 33875-33882.
20. W. Liu, S. J. Xiao and Z. Wang, *Chin. J. Process. Eng.*, 17 (2017) 119-122.
21. A. Leško and E. Navara, *Mater. Character*, 36(1996) 349-356.
22. J. G. Yang and C. P. Wu, *J. Mater. Sci. Eng.*, 2(2007) 294-298.
23. J. A. Leiro, M. H. Heinonen, T. Laiho and I. G. Batirev, *J. Electron. Spectrosc. Relat. Phenom.*, 128(2003) 205-213.
24. A. Celzard, J. F. Mareche and G. Furdin, *Carbon*, 40(2002) 2713-2718.
25. N. V. Beck, S. E. Meech, P. R. Norman and L. A. Pears, *Carbon*, 40(2002) 531-540.
26. C. E. Lu, N. W. Pu, K. H. Hou and C. C. Tseng, M. D. Ger, *Appl. Surf. Sci*., 282(2013) 544-551.
27. A. Furlan, U. Jansson, J. Lu, L. Hulman and M. Magnuson, *J. Phys. Condens. Matter*, 27(2015) 1-9.
28. H. Li, Metallurgical principle, Science press, Beijing, China, 2015.
29. C. S. Fu, Nonferrous metallurgy principle, Metallurgical industry press, Beijing, China, 1993.
30. H. Liu, N. Sun, X. Ning and H. Zhu, *J. Chin. Rare. Earth. Soc.,* 28(2010) 177-180.
31. Q. Weng, Z. Zhou, H. Lin, J. Yuan and T. Yuan, *Mat. Sci. Eng. Pow. Metall*, 1(2010) 70-73.